

Reaction  $\pi^-p \rightarrow \eta n$  at High Energies\*

O. I. Dahl, R. A. Johnson, R. W. Kenney, and M. Pripstein  
*Lawrence Berkeley Laboratory, Berkeley, California 94720*

and

A. V. Barnes, D. J. Mellema, A. V. Tollestrup, and R. L. Walker  
*California Institute of Technology, Pasadena, California 91125*  
 (Received 21 April 1976)

Measurements on the reaction  $\pi^-p \rightarrow \eta n$  have been carried out at Fermilab with beam energies from 20 to 200 GeV in the same experiment in which pion charge-exchange scattering was studied. The differential cross sections have a pronounced dip in the forward direction. The data can be described well by a simple Regge-pole model but the resulting  $A_2$  trajectory is not degenerate with the  $\rho$  trajectory extracted from the charge-exchange data.

The reaction  $\pi^-p \rightarrow \eta n$  is a companion to pion charge-exchange scattering, both theoretically and experimentally. From the theoretical point of view, these reactions are believed to be exceptionally simple so that they play a special role in the study of strong-interaction dynamics, as discussed in the preceding Letter.<sup>1</sup> Experimentally, if one observes the  $\eta$ 's via their  $2\gamma$  decays, the two reactions differ only in the  $2\gamma$  mass so that they can be easily studied in the same experiment. This has been done in previous work on this subject.<sup>2-4</sup>

The experiment is simple in principle; one requires a  $\gamma$ -ray detector capable of identifying  $\pi^0$ 's and  $\eta$ 's and measuring their angle of emission, and an efficient means of eliminating background from other reactions such as  $\pi^-p \rightarrow \pi^0 N^*$ ,  $N^* \rightarrow \pi^0 n$ . These basic needs impose severe requirements which must be met in the design of the apparatus. At 100 GeV, for example, the charge exchange cross section is  $10^{-4}$  times the total cross section for all  $\pi^-p$  interactions and  $10^{-1}$  times the cross section for producing all-neutral final states. The cross section for the  $\eta$  reaction followed by  $\eta \rightarrow 2\gamma$  decay is another factor of 10 smaller.

The experimental arrangement is shown schematically in Fig. 1. Pions in the incoming beam are tagged by a threshold Cherenkov counter and their path is measured by scintillation-counter hodoscopes, one near the target and the other approximately 60 m upstream.<sup>5</sup> The liquid-hydrogen target (length 20, 40, or 60 cm) is surrounded, except for a beam-entrance hole, by scintillation counters which veto all events with one or more charged particle in the final state. Outside these charged-veto counters is a "veto house"

designed to be very efficient for  $\gamma$  rays from  $N^* \rightarrow \pi^0 n$  and other background reactions but insensitive to recoil neutrons from the charge exchange and  $\eta$  reactions. The veto-house counters are made of Pilot 425 Cherenkov plastic sandwiched with lead sheets. Additional lead-scintillator shower counters,  $V_1, V_2, V_3, V_4$ , cover the remaining solid angle except for that subtended by the detector.

The detector [Fig. 1(b)] is a hodoscope shower detector developed for this experiment.<sup>6</sup> Photons from  $\pi^0, \eta$ , or other particle decays produce showers in a set of nineteen parallel lead plates

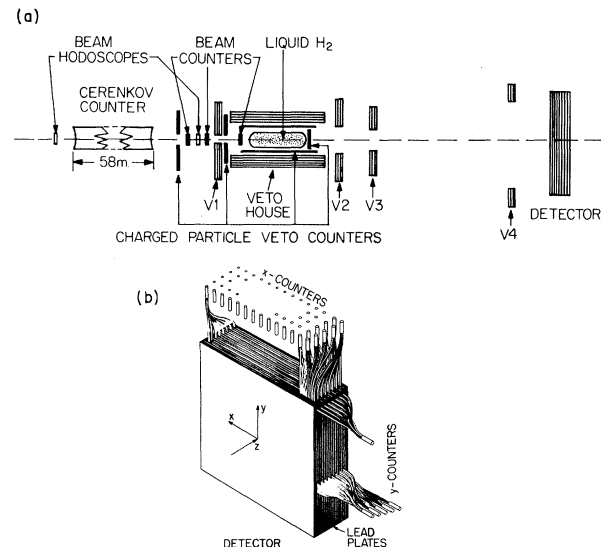


FIG. 1. (a) Schematic arrangement of the experimental apparatus (not to scale). The distance between hydrogen target and detector was scaled with energy:  $L = (16 \text{ m})(E/100 \text{ GeV})$ . The location and window openings of  $V_2, V_3$ , and  $V_4$  were adjusted accordingly. (b) The detector.

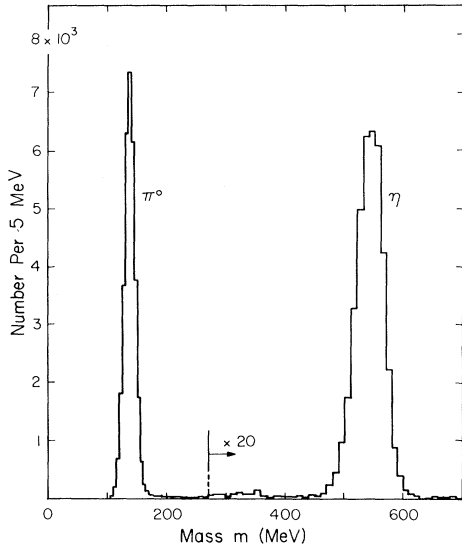


FIG. 2. Mass histogram for two-photon events from the 64.4-GeV data. The events comprising this histogram have passed all cuts used to define charge-exchange scattering or the  $\pi^-p \rightarrow \eta n$  reaction with the exception of the mass cuts.

normal to the direction of the beam, each plate being 1.12 radiation lengths in thickness and 75

cm square. Gaps between the lead plates are filled (except for the two end gaps) with scintillation plastic rods 1.05 cm wide, oriented vertically and horizontally in alternate gaps. Eight scintillation rods with the same  $x$  or  $y$  coordinate ( $z$  is along the beam direction;  $y$  is up) are connected optically by curved light pipes at one end and form one counter. A number of special tricks have been employed in the construction of these counters in order to achieve a pulse-height uniformity over their full length of approximately  $\pm 3\%$ . There are 70  $x$  counters and 70  $y$  counters, whose pulse heights give the  $x$  and  $y$  distributions of the energy deposited by all photons hitting the detector.

The moments of these energy distributions may be used to obtain the combined energy ( $E$ ), weighted mean position ( $x, y$ ), and invariant mass ( $m$ ) of the detected photons.<sup>7</sup> Typical uncertainties in the determination of these quantities are  $\sigma_E \approx 4\%$ ,  $\sigma_x \approx 1$  mm for  $\pi^0$ , and  $\sigma_m \approx 7\%$  for  $\pi^0$ , 4.5% for  $\eta$ . A mass histogram showing  $\pi^0$  and  $\eta$  peaks for the 64.4-GeV data of the present experiment is illustrated in Fig. 2.

In taking data we selected neutral final-state

TABLE I. Differential cross sections in  $\mu b/\text{GeV}^2$  and other results for  $\pi^-p \rightarrow \eta n$ ,  $\eta \rightarrow 2\gamma$ . These data have been corrected for the effects on instrumental  $t$  resolution and finite bin widths. Only statistical errors and errors in  $t$ -dependent corrections are given for  $d\sigma/dt$  but all systematic errors are included in the integral cross sections  $\sigma_I$ . The right-hand column,  $\alpha^*(t)$ , contains values of the trajectory obtained by fitting the data at each value of  $t$  separately.

-t (GeV <sup>2</sup> )	Bin Width (GeV <sup>2</sup> )	Beam Momentum in GeV						$\alpha^*(t)$
		20.8	40.8	64.4	100.7	150.2	199.3	
0.004	0.008	8.3 ± 1.0	3.14 ± 0.36	1.65 ± 0.20	0.98 ± 0.12	0.63 ± 0.08	0.46 ± 0.06	0.364 ± 0.036
0.012	0.008	8.5 ± 1.0	4.94 ± 0.46	1.82 ± 0.22	1.15 ± 0.14	0.74 ± 0.09	0.42 ± 0.06	0.333 ± 0.031
0.020	0.008	11.1 ± 1.2	3.87 ± 0.41	1.93 ± 0.23	1.41 ± 0.15	0.60 ± 0.08	0.69 ± 0.08	0.343 ± 0.034
0.032	0.016	10.2 ± 0.8	4.19 ± 0.31	2.24 ± 0.17	1.09 ± 0.09	0.84 ± 0.07	0.57 ± 0.05	0.355 ± 0.023
0.050	0.020	12.1 ± 0.8	4.52 ± 0.28	2.40 ± 0.16	1.31 ± 0.09	0.82 ± 0.06	0.55 ± 0.04	0.319 ± 0.019
0.070	0.020	11.0 ± 0.7	4.73 ± 0.28	2.56 ± 0.17	1.41 ± 0.09	0.82 ± 0.06	0.54 ± 0.04	0.335 ± 0.018
0.090	0.020	12.8 ± 0.8	4.70 ± 0.28	2.22 ± 0.16	1.42 ± 0.09	0.89 ± 0.06	0.56 ± 0.04	0.320 ± 0.019
0.110	0.020	12.3 ± 0.8	4.80 ± 0.29	2.09 ± 0.15	1.18 ± 0.09	0.61 ± 0.05	0.50 ± 0.04	0.261 ± 0.020
0.140	0.040	11.0 ± 0.5	4.22 ± 0.20	2.10 ± 0.11	1.08 ± 0.06	0.65 ± 0.04	0.447 ± 0.028	0.285 ± 0.015
0.180	0.040	9.9 ± 0.5	3.76 ± 0.18	1.68 ± 0.10	0.94 ± 0.06	0.423 ± 0.030	0.331 ± 0.024	0.226 ± 0.016
0.220	0.040	8.5 ± 0.5	2.99 ± 0.17	1.48 ± 0.09	0.73 ± 0.05	0.357 ± 0.028	0.229 ± 0.020	0.204 ± 0.017
0.260	0.040	7.4 ± 0.4	2.30 ± 0.14	1.15 ± 0.08	0.54 ± 0.04	0.236 ± 0.023	0.153 ± 0.016	0.147 ± 0.020
0.310	0.060	5.56 ± 0.32	1.84 ± 0.11	0.78 ± 0.06	0.344 ± 0.027	0.170 ± 0.016	0.091 ± 0.010	0.105 ± 0.019
0.370	0.060	3.91 ± 0.26	0.97 ± 0.07	0.47 ± 0.04	0.208 ± 0.021	0.105 ± 0.012	0.065 ± 0.009	0.094 ± 0.026
0.450	0.100	2.23 ± 0.15	0.64 ± 0.05	0.279 ± 0.025	0.109 ± 0.012	0.052 ± 0.007	0.024 ± 0.004	0.033 ± 0.025
0.550	0.100	1.16 ± 0.11	0.27 ± 0.03	0.117 ± 0.016	0.046 ± 0.008	0.0166 ± 0.0038	0.0100 ± 0.0028	-0.042 ± 0.039
0.700	0.200	0.47 ± 0.05	0.093 ± 0.013	0.033 ± 0.006	0.0134 ± 0.0031	0.0037 ± 0.0014	0.0020 ± 0.0009	-0.178 ± 0.053
0.900	0.200	0.102 ± 0.023	0.019 ± 0.006	0.006 ± 0.003	0.0034 ± 0.0016	0.0016 ± 0.0009	0.0012 ± 0.0007	-0.068 ± 0.128
1.100	0.200	0.031 ± 0.012	0.011 ± 0.004	0.0027 ± 0.0018	0.0015 ± 0.0010	0.0012 ± 0.0008	0.0002 ± 0.0003	-0.012 ± 0.156
$\frac{d\sigma}{dt}(t=0)$ from fit		6.71	2.88	1.62	0.92	0.558	0.391	
$\sigma_I(\mu b) = \int_{-1.5}^0 \frac{d\sigma}{dt} dt$		3.85 ± 0.24	1.36 ± 0.09	0.647 ± 0.044	0.337 ± 0.021	0.184 ± 0.012	0.125 ± 0.008	
Number of events		4500	5100	3500	3300	2500	2100	

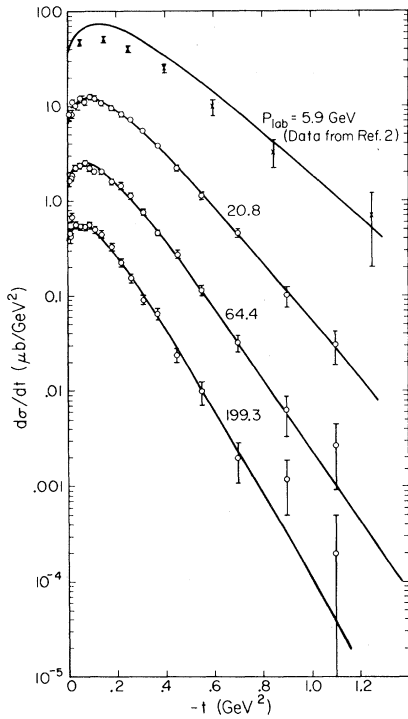


FIG. 3. Differential cross sections for the reaction  $\pi^-p \rightarrow \eta n$  with  $\eta \rightarrow 2\gamma$  at 20.8, 64.4, and 199.3 GeV from this experiment and 5.9 GeV from the experiment of Ref. 2. The curves are the result of a fit described in the text.

events using a relatively unrestrictive event trigger, recording pulse heights from nearly all counters on magnetic tape so that event-selection criteria could be studied and adjusted later in the off-line analysis. For example, none of the  $\gamma$ -ray veto counters were used in the trigger logic so that pulse-height data from these counters for all-neutral final-state events are available for use in investigating their behavior.

Many "cuts" and corrections have been applied to the data. Fortunately it has been possible to study most of these by using the data collected in the experiment and considerable effort has been

$$\alpha_0 = 0.371 \pm 0.008, \quad \alpha_1 = 0.79 \pm 0.04, \quad \alpha_2 = 0.03 \pm 0.04, \quad C_1 = 306 \pm 27, \quad C_2 = -9800 \pm 800, \quad b = 3.80 \pm 0.31.$$

The units are such that  $t$  is in  $\text{GeV}^2$ ,  $\nu$  in  $\text{GeV}$ , and  $d\sigma/dt$  in  $\rho\text{b}/\text{GeV}^2$ . This fit gives  $\chi^2 = 109$  for 108 degrees of freedom. Curves calculated from the above expression are shown in Fig. 3 including an extrapolation to 5.9 GeV for comparison with the lower-energy data.<sup>2</sup> The above parametrization, obtained by fitting to our data alone,

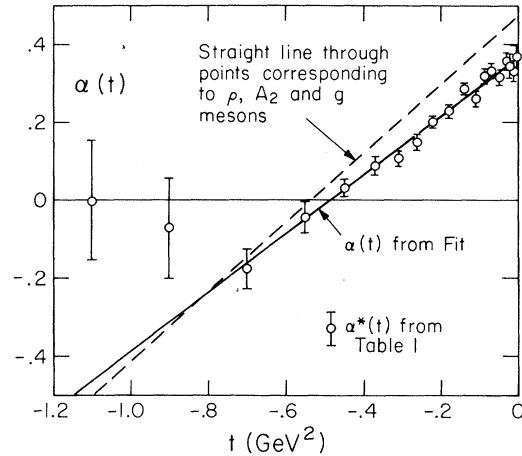


FIG. 4. The effective trajectory  $\alpha(t)$ .

devoted to this investigation.

The results of our measurements for the reaction  $\pi^-p \rightarrow \eta n$  ( $\eta \rightarrow 2\gamma$ ) at energies of 20 to 200 GeV are presented in Table I. The differential cross sections at three of the six energies studied are also shown in Fig. 3. These data have been corrected for the effects of instrumental  $t$  resolution and finite  $t$  bins by the procedure described in the preceding Letter on charge-exchange scattering.<sup>1</sup>

According to Regge ideas, the  $A_2$  Regge pole is expected to dominate the  $\eta$  reaction so that an analysis of these data should give information about the  $A_2$  trajectory. As in the case of pion charge exchange, our data on  $\pi^-p \rightarrow \eta n$  can be described remarkably well by the simplest Regge-pole model with a power-law energy dependence and a nearly linear trajectory,  $\alpha(t)$ .

A good phenomenological description of our data is provided by the following parametrization<sup>1</sup>:

$$\frac{d\sigma(s, t)}{dt} = \beta(t)\nu^{2\alpha(t)-2}, \quad (1)$$

with  $\alpha(t) = \alpha_0 + \alpha_1 t + \alpha_2 t^2$ ,  $\beta(t) = (C_1 + C_2 t)e^{bt}$ , and  $\nu = (s - u)/4M$ . The following values for the parameters have been found by a fit:

agrees only qualitatively with the lower-energy data.

The trajectory  $\alpha(t)$  obtained from the fit is shown by the solid curve in Fig. 4, along with "data points,"  $\alpha^*(t)$ , obtained in the conventional manner by fitting to the data at each value of  $t$

separately, using the form (1). According to the idea of exchange degeneracy, the  $A_2$  and  $\rho$  trajectories should be the same. Our results show that they are not, in agreement with a conclusion already reached from the previous experiments. In comparison with the  $\rho$  trajectory obtained from the charge-exchange data, the  $A_2$  trajectory found above has a smaller intercept  $\alpha_0$  and a smaller slope  $\alpha_1$  at  $t=0$ .

\*Work supported in part by the U. S. Energy Research and Development Administration. Prepared under Contract No. E(11-1)-68 at California Institute of Technology and Contract No. W-7405-ENG-48 at Lawrence Berkeley Laboratory.

<sup>1</sup>A. V. Barnes *et al.*, preceding Letter [Phys. Rev. Lett. **37**, 76 (1976)].

<sup>2</sup>O. Guisan *et al.*, Phys. Lett. **18**, 200 (1965).

<sup>3</sup>M. A. Wahlig and I. Mannelli, Phys. Rev. **168**, 1515 (1968).

<sup>4</sup>V. N. Bolotov *et al.*, Nucl. Phys. **B73**, 387 (1974).

<sup>5</sup>At 20 GeV the upstream beam hodoscope was removed in order to minimize multiple scattering, and the Cherenkov counter was used to eliminate electrons rather than to tag pions.

<sup>6</sup>The detector will be described elsewhere in greater detail: A. V. Barnes, A. V. Tollestrup, and R. L. Walker, to be published.

<sup>7</sup>The moments algorithms were developed while planning the experiment. They are described in the reports listed under Ref. 1 of the preceding Letter (Ref. 1) on charge-exchange scattering.

## Polarization Measurements around the Secondary Dip in $\pi p$ Elastic Scattering\*

P. Auer, R. Giese, D. Hill, K. Nield, P. Rynes, B. Sandler, and A. Yokosawa  
*Argonne National Laboratory, Argonne, Illinois 60439*

and

A. Beretvas, G. Hicks,† D. Miller, and C. Wilson  
*Northwestern University, Evanston, Illinois 60201*

(Received 16 April 1976)

Polarization in  $\pi^-p$  elastic scattering, with emphasis in the region around the secondary dip and also  $\theta_{c.m.} = 90^\circ$ , has been measured at 2.93 and 3.25 GeV/c. We observe an interesting sign change in this angular region.

Earlier polarization measurements<sup>1,2</sup> in  $\pi p$  elastic scattering up to  $|t| \approx 2.0$  have shown the remarkable fact that, in this  $|t|$  range,  $P(\pi^+p) \approx -P(\pi^-p)$ . In terms of  $t$ -channel quantum numbers, the above results are due to interference between  $I=0$  and  $I=1$  exchange; ( $I=0$ )  $\mp$  ( $I=1$ ) in  $\pi^+p \rightarrow \pi^+p$  scattering.

What will happen beyond  $|t| \approx 2.0$  is an interesting topic, particularly where a secondary dip exists near  $|t| \approx 2.8$ . The small cross section of the secondary dip<sup>3</sup> has made it difficult to measure polarization. Our program investigates polarization in  $\pi^-p$  scattering around the secondary dip and also around  $\theta_{c.m.} = 90^\circ$  at 2.93 and 3.25 GeV/c, where cross sections are large enough for statistically meaningful measurements.

The experiment was carried out at the Argonne zero-gradient synchrotron with a polarized proton target. Some of the experimental details have been briefly described before.<sup>4</sup> We measured the trajectories of the beam particles incident on the polarized target by means of proportional-wire-

chamber hodoscopes. Incident-beam intensities were typically  $5 \times 10^5$  pions per pulse. An on-line computer recorded about 100 events per pulse on tape. Proportional-wire-chamber hodoscopes measured the  $\theta$  and  $\varphi$  angles of both final-state particles. Events from  $\pi$  scattering off the free protons of the ethylene glycol target show up as peaks in the  $\theta$  angular-correlation distribution of the two final-state particles. The background under the peaks was subtracted by using noncoplanar events to establish the shape of the  $\theta$  correlation distribution.

Figure 1 shows the results of the polarization measurements at 2.93 and 3.25 GeV/c, together with differential-cross-section data<sup>5,6</sup> at 3.0 GeV/c. The errors are statistical and include the uncertainty in background subtraction. Because of uncertainty in the target polarization, which was about 0.85 during the experiment, there is an additional normalization error of  $\pm 5\%$ .

The most interesting feature of the data is in the sign change near the position of secondary dip